Macromolecules

ARTICLE

pubs.acs.org/Macromolecules

New Approach to the Synthesis of Exfoliated Polymer/Graphite Nanocomposites by Miniemulsion Polymerization Using Functionalized Graphene

Hussein M. Etmimi* and Ronald D. Sanderson

UNESCO Associated Centre for Macromolecules & Materials/Department of Chemistry and Polymer Science, University of Stellenbosch, Private Bag X1, 7602 Matieland, South Africa

Supporting Information

ABSTRACT: A new method is described for the synthesis of exfoliated polymer nanocomposites made with modified graphite oxide (GO) using a miniemulsion polymerization technique. GO was synthesized and then modified with a reactive surfactant, 2-acrylamido-2-methyl-1-propanesulfonic acid (AMPS), which widened the gap between the graphene layers and facilitated monomer intercalation into the GO nanogalleries. The AMPS-modified GO was emulsified in the presence of styrene and butyl acrylate monomers, a surfactant (sodium dodecylbenzenesulfonate), and a hydrophobe (hexadecane). The stable miniemulsions were polymerized to afford encapsulated poly(styrene−butyl acrylate) (poly(S−BA))/GO nanocomposite latex particles. The exfoliated structure of the nanocomposites was confirmed by X-ray diffraction (XRD) and transmission electron microscopy (TEM). TEM revealed that graphene oxide nanosheets were largely exfoliated (about 2−5 nm thick) in the resultant films obtained from the synthesized nanocomposite latices. Examination of the nanostructure of the obtained nanocomposites by XRD analysis confirmed the formation of exfoliated graphene oxide nanoplatelets. The thermal stability and mechanical properties of the nanocomposites were evaluated by thermogravimetric analysis (TGA) and dynamic mechanical analysis (DMA). TGA showed that all the prepared nanocomposites exhibited enhanced thermal stability relative to the neat poly(S−BA) copolymer. DMA also revealed that the glass transition temperature of poly(S−BA) in the nanocomposites increased significantly in the presence of modified GO relative to pure copolymer. Furthermore, the nanocomposites had improved storage and loss modulus only at relatively high GO content (i.e., 5 and 6 wt % relative to monomer).

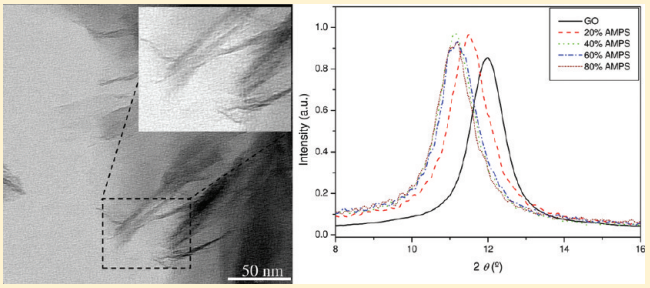

1. INTRODUCTION

Graphite is naturally abundant and well-known to be a layered material with unique and unusual properties.[1,2] It is a pseudo-two-dimensional solid with sp^2-hybridized carbon atoms arranged in a hexagonal pattern within each layer. These layers, known as graphene,[3] are organized in the ABAB alternating stacking sequence, with strong covalent bonding between the carbon atoms in the same graphene layers. Thus, cleavage of the bonds between the carbon atoms among these layers is very difficult. This results in graphene sheets having very high strength as well as good mechanical properties in the same plane.[4,5] On the contrary, the weak van der Waals interactions acting between the graphene layers makes the cleavage of bonds between these layers very easy. Therefore, graphite can be converted into high aspect ratio (length-to-thickness ratio) reinforcement platelets with nanometer-scale thickness through a process of intercalation and exfoliation.[6]

Pristine unmodified graphite cannot be easily dispersed in a polymer matrix.[7] Thus, there are very few reports of polymer nanocomposites based on pristine natural graphite.[8] This is because there are no reactive groups on the natural graphene layers, which makes it difficult for organic molecules or monomers to be loaded on its surface. In addition, graphene layers lack the affinity and space for hydrophilic or hydrophobic molecules and polymers to intercalate into its galleries. Hence, pristine graphite is usually functionalized in order to be used for the synthesis of polymer nanocomposites.[3,9] Oxidation of graphite followed by exfoliation, either by rapid thermal expansion[10] or by ultrasonic dispersion,[11] is one approach that can be used to obtain functionalized and exfoliated graphite sheets. The first synthesis of such modified graphite sheets was described by Brodie in 1859.[12] Today there are three main methods for the preparation of graphite oxide (GO) from natural graphite—as described by Brodie,[12] Staudenmaier,[13] and, more recently, Hummers and Offeman.[14] Each method is based on the oxidation of graphite in the presence of a strong concentrated mineral

Received: February 10, 2011
Revised: August 16, 2011
Published: October 17, 2011

acid (e.g., sulfuric acid) and strong oxidizing agent (e.g., potassium permanganate).

The oxidation chemistry is similar to that used to functionalize carbon nanotubes (CNTs) and results in a variety of oxygen-containing functionalities (e.g., epoxide, −OH and −COOH) at different sites on the graphite surface.[9] It is generally believed that the epoxide and hydroxyl functional groups are located in the basal planes of the graphene sheets, while the edges of these sheets are functionalized with carbonyl and carboxyl groups.[15−18]

After oxidation, GO still possesses a layered structure, but it is much lighter in color than pristine graphite due to the loss of electronic conjugation caused during the oxidation step. The oxygen-containing functionalities alter the chemistry of the graphite sheets and render them hydrophilic, thus facilitating their hydration and exfoliation in aqueous media.[19] As a result, GO easily forms stable colloidal dispersions of thin graphene oxide nanosheets in water.[20−22] The nanometer-scale sheets and galleries in the final GO, caused by the exfoliation process, as well as the oxygen groups on the edges and borders of sheets (generated by chemical oxidation) create favorable conditions that allow for suitable polymers (water-soluble) to intercalate and form polymer/GO nanocomposites.[23] However, water-insoluble (hydrophobic) monomers or polymers such as polystyrene (PS) and poly(methyl methacrylate) (PMMA) cannot be easily intercalated between GO layers.[24] This is because the GO nanosheets are hydrophilic[19] and therefore incompatible with hydrophobic monomers or polymers.[25] Thus, the compatibility between the GO nanosheets and the monomers or polymers selected for use needs to be enhanced.

In a recent study, Hu et al.[26] reported the use of GO for the synthesis of PS nanocomposites by *in situ* emulsion polymerization. The authors showed that this could be a promising route for the production of composite materials based on graphite with improved thermal stability. However, during the synthesis procedure the GO was reduced to graphite using hydrazine hydrate, which decreased the hydrophilic nature of graphite sheets, leading to better compatibility with monomer. In another study, Wang and Pan[24] reported that the intercalation of monomer, followed by *in situ* polymerization, occurred during the emulsion polymerization of methyl methacrylate in the presence of GO. The authors observed that the mechanical properties of the composites (i.e., notched Izod impact strength and tensile strength) decreased as the content of GO increased from 1 to 8 wt %. They attributed this phenomenon to low compatibility of GO with PMMA, which resulted in composites with intercalated structure. They also showed that the amount of PMMA that grafted onto GO was very small, and the surface properties of GO were little improved.

Graphite-derived materials such as GO have been widely used as fillers for the preparation of polymer nanocomposites to improve their mechanical, thermal, and electrical properties.[25,27−29] Methods such as solution blending,[30] exfoliation−adsorption,[31] melt intercalation,[32] and *in situ* intercalation[33] polymerization have been used to prepare such nanocomposites. However, there are still many challenges (e.g., the preparation method) that must be addressed before such nanocomposites can reach their full potential. Although significant success has been achieved in the preparation of polymer/graphite nanocomposites using *in situ* polymerization of the monomer in the presence of graphite,[28,33,34] there are only few reports on the preparation of these composites in emulsion systems. In particular, the use of miniemulsion polymerization has not been investigated for the synthesis of such nanocomposites.

Miniemulsion polymerization can be a very useful method for the preparation of nanoscale latex particles made with filler materials such as graphite. This is due to the initial dispersion of the polymerization reaction components, which can be directly polymerized into polymer particles. In the miniemulsion process, the oil phase, which consists of the monomer and the filler, can be dispersed in the water phase by a high-shear device such as a sonicator. This will lead to the formation of monomer droplets containing the filler particles and stabilized by the surfactant and the hydrophobe from which polymer particles will develop during the polymerization step.[35] In various studies, miniemulsion polymerization was successfully used for the incorporation of filler compounds such as clay[35] and CNTs[36] within a polymer matrix. In a previous study, we investigated the use of RAFT polymerization for the synthesis of PS/GO nanocomposites.[37] GO was prepared and successfully immobilized using dodecyl isobutyric acid trithiocarbonate as RAFT agent. The resultant RAFT-attached GO was used for the preparation of PS/GO nanocomposites in a controlled manner using miniemulsion polymerization. The study showed that miniemulsion could be used as effective method for the synthesis of graphite-based polymer nanocomposites with improved properties.

In an emulsion system there are three possible nucleation mechanisms for the growing oligomeric radical species: micellar, homogeneous (water phase), and, less often, droplet nucleation.[38] Droplet nucleation occurs when radicals formed in the aqueous phase enter monomer droplets and propagate to form polymer particles. In miniemulsion polymerization droplet nucleation is the predominant mechanism of particle formation due to the small size of the monomer droplets and the presence of few or no micelles in the system.[39] These submicrometer droplets have a large interfacial area and are capable of capturing most of the oligomeric free radicals—thus, the droplets become the locus of nucleation. The incorporation of filler materials is much easier in miniemulsion than in conventional emulsion polymerization because the need of mass transport through the water phase is minimized by droplet nucleation.

Miniemulsions contain submicrometer-sized monomer droplets ranging from 50 to 500 nm.[40,41] The droplets are formed by shearing a premixed system comprising water, monomer, surfactant, and a hydrophobe (also referred to as a cosurfactant or a costabilizer). The surfactant prevents the droplets from coalescing and the hydrophobe prevents Ostwald ripening. The first report on miniemulsion polymerization dates back to 1973, when Ugelstad et al.[42] reported the polymerization of styrene (St) in the presence of a mixed emulsifier system of sodium dodecyl sulfate and cetyl alcohol.

Miniemulsion polymerization offers several advantages over other dispersion polymerization techniques,[41] such as a small particle size of the final latex particles, efficient use of surfactant, and production of lattices with high solids content. The particles that can be produced are a 1:1 copy of the miniemulsion droplets.[43,44] The latter can be attributed to the fact that the miniemulsion droplets are directly polymerized to polymer particles.[43] This method can also be used for the polymerization of hydrophobic monomers with low water solubility, which often can only be polymerized (with difficulty) in emulsion polymerization.[45,46] The advantages of miniemulsion polymerization make it attractive to be used for the synthesis of polymer/graphite nanocomposites.

In several studies authors have focused on investigating the intercalation of clay with reactive surfactants (known as surfmers),

such as 2-acrylamido-2-methyl-1-propanesulfonic acid (AMPS), to prepare polymer−clay nanocomposites (PCNs).[47−49] The use of this compound as a clay modifier seems to play a major role in achieving successful exfoliation of clay in the synthesized PCNs. Xu et al.[47] used AMPS as a clay modifier in the synthesis of exfoliated poly(styrene-*co*-methyl methacrylate)/clay nanocomposites using emulsion polymerization. They found that AMPS has the ability to increase the interlayer spacing between clay layers from 1.17 nm in pristine clay up to 2.1 nm, depending on the AMPS/clay ratio used. They also found that AMPS can accelerate the insertion of comonomers into clay layers, resulting in PCNs with exfoliated structures.

It is believed that the interaction of AMPS with clay occurs by adsorption of AMPS on the surface of the clay by formation of hydrogen bonds between the sulfate and amido groups of AMPS with the hydroxyl groups on the clay surface.[50] The same concept can be applied to GO, since GO has a larger *c*-axis spacing compared to the pristine graphite, and polar groups such as hydroxyl and carboxylic groups on its surface. Thus, the intercalation of AMPS into GO particles becomes possible via the formation of hydrogen bonds between the functional groups of AMPS and GO.

Here we report a new method for the synthesis of exfoliated poly(styrene−butyl acrylate)/GO (poly(S−BA)/GO) nanocomposites using the miniemulsion technique. First, the GO sheets were modified with the reactive surfactant, AMPS. The resultant modified GOs were then used in the synthesis of poly(S−BA) nanocomposites using *in situ* miniemulsion polymerization to promote the intercalation of water-insoluble monomers, St and butyl acrylate (BA), within layered GO. We intend to show that AMPS can intercalate into the GO galleries and lead to an increase in the interlayer spacing (commonly known as the *d*-spacing) between graphene oxide nanosheets. Furthermore, due to its polymerizable groups, AMPS can take part in the polymerization of St and BA and thus provide the exfoliation driving force for the formation of nanocomposites with exfoliated structure.

To the best of our knowledge, this is the first report on the modification of GO with a surfmer such as AMPS and the subsequent use of the modified GOs in the miniemulsion polymerization of St and BA monomers. The treatment of GO with organic modifiers such as AMPS could lead to the synthesis of chemically modified GO derivatives possessing improved properties. The modification with AMPS will alter the intercalation behavior of GO and allow for the complete exfoliation of GO into individual graphene oxide nanosheets in polymer systems. The use of miniemulsion will also allow the formation of polymer particles, containing the modified graphene oxide nanosheets, which can be polymerized in a convenient one-step nanoincorporation process.

2. METHODS: EXPERIMENTAL AND CHARACTERIZATION

2.1. Materials. Styrene (99%, Aldrich) and butyl acrylate (99%, Aldrich) were purified by washing with aqueous 0.3 M KOH, followed by distillation at 40 °C under reduced pressure. Sodium dodecylbenzene sulfonate (SDBS) (99%, Fluka), 2-acrylamido-2-methyl-1-propanesulfonic acid (99%, Aldrich), and hexadecane (HD) (99%, Sigma-Aldrich) were used as received. Potassium persulfate (KPS) was obtained from Aldrich and purified by recrystallization from methanol. Potassium permanganate (99%), sodium nitrate (99%), and hydrogen peroxide (30%) were obtained from Sigma-Aldrich and used as received. Sulfuric acid (98.08%, Merck) was used as received. Distilled and deionized (DDI) water was obtained from a Millipore Milli-Q water purification system. Expanded graphite (99.5%) was obtained from Graphit Kropfmühl AG (Hauzenberg, Germany) and used without any further purification. GO was prepared as described in the literature, with some modification.[14]

2.2. Preparation of GO. GO was prepared by treating the natural graphite with potassium permanganate in the presence of sulfuric acid, following the method of Hummers and Offeman.[14] In brief, powdered flake graphite (10 g) and sodium nitrate (5 g) were stirred into 98% sulfuric acid (230 mL). As a safety measure, the ingredients were mixed in a 1.5 L flask that was previously cooled to 0 °C in an ice bath. Potassium permanganate (30 g) was slowly added to the suspension, while maintaining vigorous agitation, taking care not to allow the temperature of the suspension to exceed 20 °C. The ice bath was then removed, and the temperature of the suspension was brought to 35 °C, where it was maintained for 30 min. The mixture gradually thickened as the reaction progressed, and after 30 min the mixture became pasty, with a brownish-gray color. DDI water (460 mL) was then slowly stirred into the paste, causing a violent reaction and an increase in temperature to 100 °C. The diluted suspension was maintained at this temperature for 15 min. The suspension was then further diluted with warm water (∼420 mL) and hydrogen peroxide (3%) (100 mL) to reduce the residual permanganate and manganese dioxide to colorless soluble manganese sulfate. Upon treatment with the peroxide, the suspension turned bright yellow. Filtration afforded a yellow-brown filter cake. The GO was washed several times with DDI water until neutrality. The final solid containing the GO platelets was obtained by centrifugation.

2.3. Modification of GO with AMPS. GO was treated with AMPS as follows: GO (0.5 g) was introduced to a 250 mL flask containing DDI water (150 g). The mixture was stirred at room temperature for 15 min, after which it was sonicated using a Vibracell VCX 750 ultrasonicator (Sonics & Materials) for a further 15 min. This was done in order to achieve complete dispersion of GO nanosheets in water. AMPS was added to the mixture (20 wt % relative to GO), which was then stirred for a further 24 h at room temperature. The treatment was repeated with various quantities of AMPS: 40, 60, and 80% relative to GO.

2.4. Typical Preparation of Poly(S−BA)/GO Using Miniemulsion Polymerization. The AMPS-treated GO (AMPS-GO) (modified with 40% AMPS) was added to the monomer mixture (St and BA), and the mixture was stirred for 1 h to allow effective swelling of GO with the monomers. Surfactant (∼2 wt % SDBS relative to monomer) and HD were added, and the mixture was stirred for a further 30 min. The mixture was sonicated using a Vibracell VCX 750 ultrasonicator (Sonics & Materials) for 10 min to obtain the miniemulsion latex. The sonicator amplitude was set at 80%, and the pulse rate was set at 2 s. The average energy expended was ∼67 kJ. A three-neck round-bottomed flask containing the resultant miniemulsion latex was then immersed in an oil bath at room temperature. KPS (0.008 g) was added, and the contents of the flask were nitrogen purged for 15 min before increasing the temperature to 70 °C to start the polymerization. The reaction was carried out for 4 h under a nitrogen atmosphere, after which it was cooled to room temperature to stop the polymerization.

A similar procedure was followed for the synthesis of a poly(S−BA) standard without GO by miniemulsion polymerization. The oil phase, consisting of St and BA monomers, and HD, was mixed with an aqueous solution of SDBS for 30 min. The mixture was then sonicated under the same conditions used for the synthesis of poly(S−BA)/GO nanocomposites for 15 min to afford the miniemulsion latex. KPS (0.008 g) was added, and the temperature was increased to 70 °C to start the polymerization. The reaction was carried out for 4 h under a nitrogen atmosphere. The various formulations used for the polymerization of

Table 1. Quantities of Reagents and Monomers Used in the Miniemulsion Polymerization Reactions

nanocomposite	AMPS-GO (g)	St (g)	BA (g)	SDBS (g)	HD (g)
P(S−BA)		4.51	0.51	0.102	0.022
P(S−BA)/GO-1	0.05	4.51	0.50	0.105	0.023
P(S−BA)/GO-2	0.10	4.50	0.52	0.101	0.022
P(S−BA)/GO-3	0.15	4.56	0.44	0.102	0.024
P(S−BA)/GO-4	0.20	4.51	0.50	0.105	0.023
P(S−BA)/GO-5	0.25	4.50	0.51	0.104	0.022
P(S−BA)/GO-6	0.30	4.50	0.52	0.101	0.022

poly(S−BA)/GO nanocomposites and the poly(S-BA) standard are tabulated in Table 1.

2.5. Analytical Techniques. Various analytical techniques were used to characterize the GO samples and the poly(S−BA)/GO nanocomposites (i.e., powder). Nanocomposite samples were obtained from the latex by precipitation. The latex (3 mL) was precipitated with concentrated hydrochloric acid; the precipitate was washed several times with methanol and then with DDI water and finally dried at 40 °C under reduced pressure. The analytical instrumentation and procedures used were as follows:

2.5.1. Transmission Electron Microscopy (TEM). TEM was used to directly visualize the morphology of the graphene oxide particles in poly(S−BA)/GO nanocomposites at the nanometer level. Bright field TEM images were recorded using a LEO 912 Omega TEM instrument (Zeiss, Germany) at an accelerating voltage of 120 kV. Prior to analysis, the miniemulsion samples were diluted with DDI water (0.05%) and placed on 300-mesh copper grids, which were then transferred to the transmission electron microscope.

Portions of the poly(S−BA)/GO nanocomposite miniemulsion samples were dried, embedded in epoxy resin, and then cured for 24 h at 60 °C. The embedded samples were ultramicrotomed with a diamond knife on a Reichert Ultracut S ultramicrotome at room temperature. This resulted in sections with a nominal thickness of ∼100 nm. The sections were transferred from water to 300 mesh copper grids, which were then transferred to the TEM apparatus for analysis. TEM was also used to visualize the GO particles. GO (0.1 g) was dispersed in DDI water (50 g) by sonication. The GO samples were diluted with DDI water (0.05%) and placed on 300 mesh grids for analysis. The average particle sizes and gallery spacing were calculated using computer software, ImageJ (NIH).

2.5.2. Scanning Electron Microscopy (SEM). The microstructure of the graphite flakes and sheets before and after the oxidization was observed using a scanning electron microscope (SEM, Leo 1430 VP). Samples were carefully mounted on the top of the sample holder, which was then coated with a single layer of gold in order to make the sample surface electrically conducting. The holder was loaded into the chamber of the SEM instrument, and images were recorded at between 500× and 40000× magnification at 7 kV voltage.

2.5.3. Thermogravimetric Analysis (TGA). TGA measurements were carried out on a Q500 thermogravimetric analyzer (TA Instruments). Sample sizes of less than 15 mg were used for all analyses. Analyses were carried out from ambient temperature to 900 °C, at a heating rate of 20 °C/min, under a nitrogen atmosphere (nitrogen purged at a flow rate of 50 mL/min).

2.5.4. Fourier-Transform Infrared (FT-IR) Spectroscopy. FT-IR spectra were obtained using a Nexus 470 FT-IR spectrometer (Thermo Nicolet) and recorded by averaging 32 scans. All spectra were acquired from 450 to 4000 cm^{-1} by using an attenuated total reflectance unit at a wavenumber resolution of 4 cm^{-1}.

2.5.5. Gel Permeation Chromatography (GPC). GPC analyses were carried out using a 610 fluid unit, a 410 differential refractometer at 30 °C, and a 717 plus autosampler (Waters). A 600E system controller, run by Millenium 32 V3.05 software, was used in all analyses. Tetrahydrofuran (THF; HPLC grade), sparged with helium (IR grade), was used as the eluent, at a flow rate of 1 mL/min. Two PLgel 5 μm mixed-C columns and a PLgel 5 μm guard precolumn were used. The column temperature was 35 °C, and the injection volume was 100 μL. The system was calibrated with narrow PS standards (5 mg/mL THF), ranging from 2.5 × 10^3 to 8.9 × 10^4 g mol^{-1}. The nanocomposite samples were dissolved in THF (5 mg/mL) over a period of 24 h and then filtered through a 0.45 μm nylon filter.

2.5.6. X-ray Diffraction (XRD). XRD patterns were obtained using a X'Pert PRO multipurpose diffractometer (PANalytical B.V., The Netherlands) equipped with a Cu Kα sealed tube X-ray source (wavelength 1.514 Å). X'Celerator in Bragg−Brentano mode was used as the detector throughout.

2.5.7. Dynamic Mechanical Analysis (DMA). DMA analysis of the poly(S−BA)/GO films was carried out using a Physica MCR 501 rheometer apparatus (Anton Paar, Germany). Parallel-plate geometry (25 mm diameter), with a 1 mm gap distance, and a constant strain of 0.1% were used. All measurements were carried out from 180 to 40 °C, at a cooling rate of −5 °C, an oscillation frequency of 1 Hz, and a normal force of 5 N. The nanocomposite films were prepared by pressing the composite samples into thin discs (25 mm) using a hydraulic press machine at 120 °C.

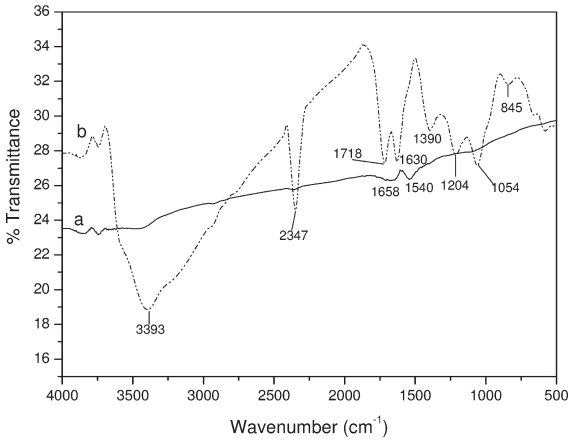

Figure 1. FT-IR spectra of (a) pristine graphite and (b) its oxidized form (GO).

3. RESULTS AND DISCUSSION

3.1. Preparation of GO. Figure 1 shows the FT-IR spectra of the pristine graphite (Figure 1a) and its oxidized form (GO) (Figure 1b). In Figure 1a the peaks at 1658 and 1540 cm^{-1} correspond to the stretching of C═C bonds in the benzene ring of graphene.[22]

Figure 1b shows the characteristic peaks of GO, such as the stretching vibration of the hydroxyl groups (−OH), the stretching vibration of the carboxyl groups (−COOH), the vibration of O−H, the vibration of C−O, and the vibration of epoxy groups, centered at 3393, 1718 and 1630, 1390, 1054, and 845 cm^{-1}, respectively.[22] The peaks at 2347 and 1630 cm^{-1} can be attributed to carbon dioxide and the deformation vibration of water molecules in the sample, respectively.[22,51] The appearance of these new oxygen-containing functional groups indicates that oxidation of the graphite sheets was achieved. Indications of the C═C bond were not found in the GO spectrum, which shows

that complete oxidation was achieved, due to the strong $KMnO_4$ oxidant used.

3.2. Characterization of GO. *3.2.1. Interlayer Spacing of GO As Determined by XRD.* The oxidation of graphite is expected to increase the interlayer distance (d-spacing) of stacked graphene.[24] XRD was used to determine the d-spacing between the graphene sheets before and after oxidation. Results showed an increase in the d-spacing between graphene sheets after oxidization. In the case of pristine graphite there is a sharp reflection peak at $2\theta = 26.4°$ in the XRD scattering pattern due to the interlayer (002) spacing ($d = 0.34$ nm).[52,53] The XRD results of pristine natural graphite and its oxidized form are shown in Figure S1 of the Supporting Information.

Upon oxidization, the characteristic peak of graphite could not be detected; the GO exhibited only one peak at a lower 2θ value = 12°. This indicates that the interlayer distance between neighboring graphene oxide layers in GO had increased (layers are now ~0.74 nm apart) because of the intercalation by functional groups and moisture.[17] The fact that the XRD pattern of GO exhibited only one peak also suggests that a highly oxidized GO sample had been synthesized (in agreement with FT-IR results).

3.2.2. Nanostructure of GO As Determined by SEM and TEM. SEM was used to visualize the graphite particles before and after oxidation. Results are shown in Figures 2 and 3. The original graphite particles have a platelike shape, with average sizes of 1−10 μm and thickness of 50−200 nm (see Figure 2). Each flake consists of multiple layers of graphene nanoplatelets with aspect ratios of about 20−50. The layers of the intercalated graphite sheets can be expanded a few hundred times during oxidation, as reported in the literature.[54] The SEM images of dried GO films show that a continuous filmlike structure is formed by elimination of water (see Figure 3a). This might be due to the platelike nanostructure—which could be very desirable for the construction of high-quality films. Furthermore, due to the presence of the oxygen-containing functional groups on the surface, GO sheets can interact with each other by hydrogen bonding, resulting in the formation of a film structure.

The GO structure is basically parallel boards, which collapse and deform during the drying process, resulting in many pores of different sizes, ranging from 300 to 800 nm. This can be seen in Figure 3b, where a higher magnification SEM image of a GO surface is presented. The thickness of the graphene oxide sheets in the exfoliated GO is in the micrometer range, as evident in the SEM image in Figure 3c.

According to the microstructure of graphite, the thickness of sheets in intercalated graphite may be as thin as a single carbon layer when the graphite is fully exfoliated. The structure of graphite, consisting of graphite nanosheets and graphene nanolayers (nanoplatelets), is illustrated in Figure 4. Figure 4a shows that the graphite flakes consist of graphite sheets, which are normally <100 nm in thickness. Each graphite sheet can be further divided into aggregates of a number of graphite nanosheets, 2−8 nm thick (see Figure 4b). These graphite nanosheets are composed of graphene nanoplatelets, which can be as thin as one carbon atom layer thick (Figure 4c).[55] TEM was used to observe the GO nanosheets (dispersed in water) at the nanometer level (see Figure 5). The TEM images clearly show that the thick graphite sheets consist of thinner nanosheets, 2−5 nm thick, and the gallery spacing between these nanosheets is about 5−10 nm (Figure 5b). The reason why SEM images showed graphite sheets with a thickness of about 1 μm is possibly the stacking and combining of graphite nanosheets on the surface during the drying process.

3.2.3. Organization of AMPS in the GO Galleries. Changes in the interlayer distance of GO can be caused by the intercalation of organic compounds. A change in the d-spacing of graphite as a function of the incorporation of different organic compounds has been reported elsewhere.[56−58] The d-spacing is calculated according to Bragg's law[59] (see eq 1):

$$2d \sin \theta = n\lambda \quad (1)$$

where d is the distance between two diffractional lattice planes of graphite, θ is the measured diffraction angle, n is the order of

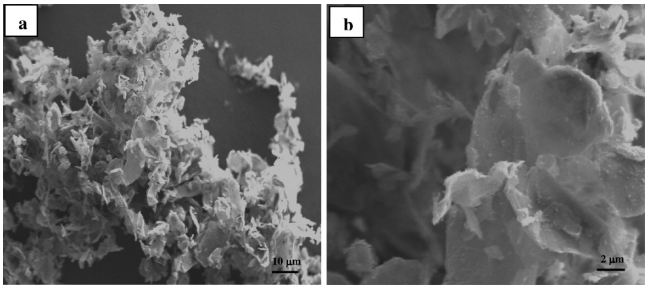

Figure 2. SEM images of natural graphite: (a) at low magnification and (b) at higher magnification.

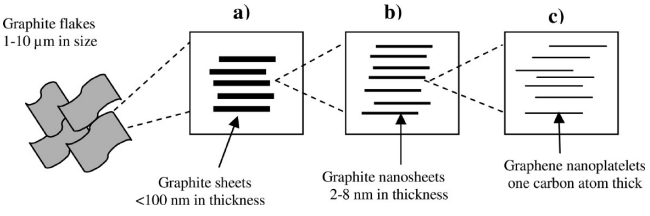

Figure 4. Microstructure of the graphite flakes and graphite nanosheets consisting of graphene nanolayers.

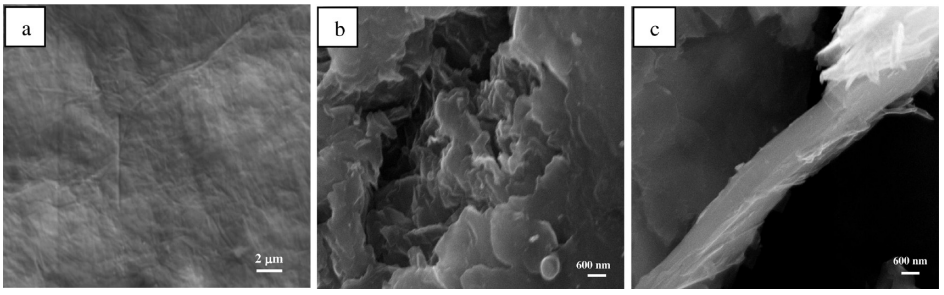

Figure 3. SEM images of GO: (a) at low magnification and (b, c) at higher magnification.

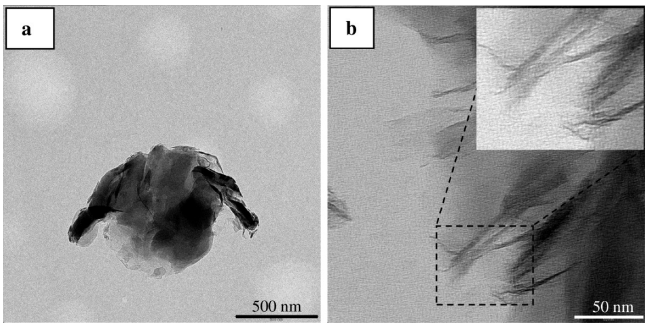

Figure 5. TEM images showing thinner sheets inside exfoliated GO: (a) low magnification image and (b) higher magnification image.

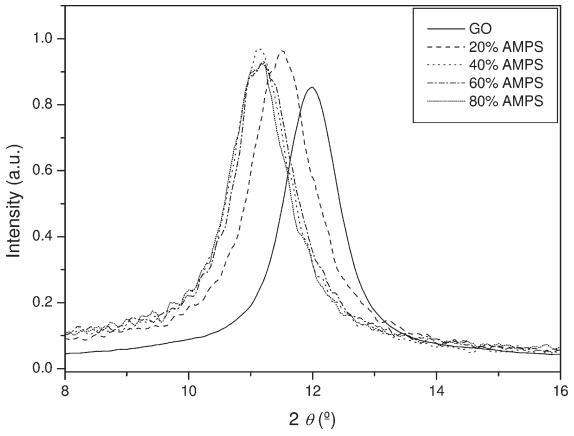

Figure 6. XRD patterns of GO and GOs modified with different quantities of AMPS.

interference, and λ is the wavelength of X-ray radiation used in the diffraction experiment.

Figure 6 shows the XRD spectra of pure GO and the GOs modified with different quantities of AMPS. Table 2 tabulates the *d*-spacing calculated from the GO peaks in the XRD spectra. The interlayer spacing of GO increased from 0 to 20% and 20 to 40% AMPS concentration but remained steady thereafter. It reached a maximum of about 0.80 nm when ≥40% AMPS was used. This was rather surprising because more AMPS molecules should lead to an increase in the interlayer spacing of GO. However, this could be explained by the fact that there are a limited number of functional groups on the surface of GO that could interact with the AMPS molecules. It could also be attributed to the nature of AMPS molecules and their arrangement inside the galleries of GO. This behavior has been reported previously for other fillers, such as clay, modified with AMPS.[50] The AMPS molecules could adopt different conformations inside the GO galleries as the AMPS concentration changes, resulting in different *d*-spacings. The AMPS molecules are thought to lie either parallel to the host layers, forming mono- or bilayers, or radiate away from the surface, forming extended (paraffin-type) mono- or bimolecular arrangements.[60]

The increase in the interlayer spacing of modified GO relative to pure GO confirmed the insertion of AMPS between graphene oxide nanosheets, not only the presence of AMPS on the external surface of the GO. The AMPS molecules can interact with GO both via their amino and sulfate groups. These groups can form hydrogen bonds with the functional groups of GO. This is in agreement with the

Table 2. Interlayer Distance (*d*-Spacing) of GO and GOs Modified with Different Amounts of AMPS

sample code	AMPS (wt %)	2θ (deg)	*d*-spacing (nm)
GO	0	12.00	0.74
AMPS-GO-1	20	11.50	0.77
AMPS-GO-2	40	11.14	0.80
AMPS-GO-3	60	11.16	0.79
AMPS-GO-4	80	11.12	0.80

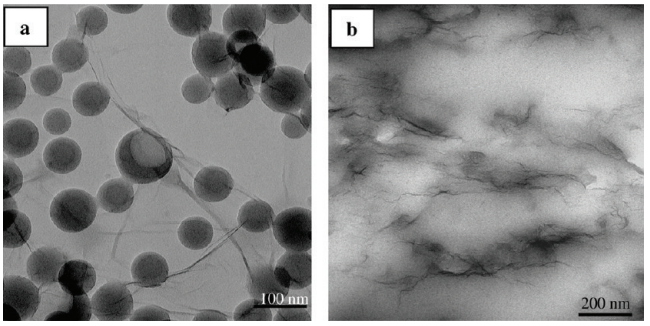

Figure 7. TEM images of poly(S−BA)/GO nanocomposite latex made with 1 wt % GO relative to monomer: (a) latex particles and (b) a microtomed film cast from the same latex.

findings of Liu et al.,[33] after they investigated the synthesis of poly(vinyl acetate)-intercalated GO by *in situ* intercalative polymerization. They prepared a graphite intercalation compound in which GO was intercalated with *n*-octanol. They attributed the interaction of GO to the formation of hydrogen bonds between the hydroxyl groups of the *n*-octanol and the other polar groups of the GO.

Greesh et al.[50] investigated the adsorption mechanism of AMPS and other related compounds into the galleries of montmorillonite clay. They found that the interaction of AMPS with clay occurs by adsorption of AMPS on the edges and the surfaces of the clay galleries. The formation of hydrogen bonds between the sulfate and amido groups of AMPS with the hydroxyl groups and water molecules adsorbed on the clay surface leads to an increase in the basal spacing of the clay. The intercalation of AMPS inside the GO galleries could be similar to that occurring in clay particles because the GO has many functional groups, such as hydroxyl and carboxyl, present on its surface.[9,22] The sulfate and amido groups of AMPS can interact with the hydroxyl and carboxyl groups present on the GO.

3.3. Characterization of Poly(S−BA)/GO Nanocomposites. *3.3.1. Determination of Morphology by TEM.* TEM was used to visually detect the latex particles that were synthesized and to determine the morphology of the films that were prepared from these latices. Figure 7 shows TEM images of the nanocomposite prepared using 1 wt % GO relative to monomer. The particle size distribution is fairly narrow, and there are many graphene oxide nanosheets outside the polymer particles, as can be seen in Figure 7a. This suggests that most of the GO sheets have not been encapsulated by the copolymer shell. This is to be expected because of the hydrophilic nature of the GO, which prefers to be in the water phase. The unmodified GO sheets contain a number of stacked graphene nanosheets with relatively

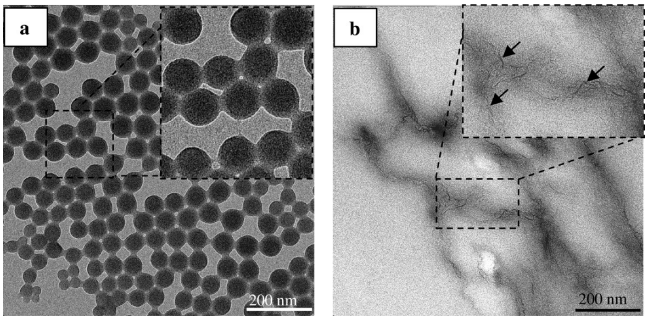

Figure 8. TEM images of poly(S−BA)/GO nanocomposite prepared using 1 wt % AMPS-modified GO: (a) latex particles and (b) a microtomed film cast from the same latex.

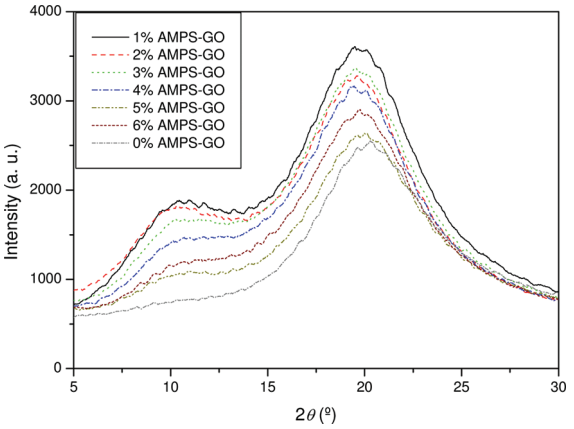

Figure 9. XRD results of poly(S−BA)/GO nanocomposites made with different amounts of AMPS-modified GO.

small *d*-spacing (see Figure 6). These stacked nanosheets are large in size compared to the polymer particles, and thus they are unable to enter the polymer particles. The graphene sheets can also be seen in a TEM image of the dried film that was embedded into the epoxy resin (Figure 7b). Most of the GO nanosheets are mainly of intercalated morphology, with the exception of some areas that contain few exfoliated graphene oxide nanoplatelets. The stacking of graphene indicates that the GO did not disperse very well in the polymer matrix, leading to the formation of an intercalated structure.

However, when GO was modified with AMPS, the graphene oxide nanosheets could not be seen in the TEM images (see Figure 8a). This absence of graphene sheets in the latex suggests that all the modified GO nanosheets were encapsulated in the copolymer particles. The modification of GO with AMPS increased the gap between the graphene platelets, resulting in largely exfoliated GO (the nanosheets are smaller in size due to exfoliation). These nanosheets can easily enter the polymer latex particles to form the core domain.

The TEM image in Figure 8a also shows that a miniemulsion with good particle size distribution was obtained. The dark core domains inside the particles can be attributed to the presence of modified GO nanosheets inside the copolymer shell layer. AMPS could also alter the chemistry of GO, resulting in modified GO with increased hydrophobicity and allowing for better compatibility between GO sheets and hydrophobic monomers (St and BA). Furthermore, the TEM images of the microtomed films that were prepared from the latex show that the AMPS-modified GO platelets were mostly of exfoliated structure. Figure 8b shows very thin graphene nanoplatelets, about 2−5 nm thick, which correspond to ∼2−5 layers stacking.[61] This indicates that most of the graphene nanosheets dispersed as a thin layer, which means that the graphene platelets are mostly exfoliated in the polymer matrix. This is due to the effect of AMPS, which widened the *d*-spacing of GO and facilitated the intercalation of monomer into the GO nanogalleries, resulting in an exfoliated structure.

Recently, Stankovich et al.[62] reported that the treatment of GO with organic isocyanates resulted in a new class of functionalized GO materials that had reduced hydrophilic properties. The authors showed that, in contrast to the as-prepared GO, the modified GO does not disperse in water. However, it can be dispersed and readily exfoliate in polar aprotic solvents such as *N*, *N*′-dimethylformamide, *N*-methylpyrrolidone, dimethyl sulfoxide, and hexamethylphosphoramide to form stable colloidal dispersions. In the current study, the effect of AMPS on the properties of GO could provide the driving force to allow better intercalation of the monomer in the GO nanogalleries. It should be noted here that in all nanocomposites the GO was modified with 40% AMPS. XRD showed that the highest change in the *d*-spacing of GO was obtained when 40% AMPS relative to GO was used. Any further increase in AMPS concentration did not change the *d*-spacing compared to the GO modified with 40% AMPS (see Figure 6). The presence of an excess amount of AMPS could have an effect on the polymerization rate,[47] and therefore the minimum amount of AMPS that led to a significant change in the *d*-spacing of GO was used (i.e., 40%).

3.3.2. Determination of Nanocomposite Structure by XRD. Figure 9 shows the XRD results of poly(S−BA)/GO nanocomposites prepared with different amounts of AMPS-modified GO. For comparison, XRD results of a poly(S−BA) standard are also included in Figure 9. The nanostructure ranged from intercalated to largely exfoliated morphology, depending on the amount of modified GO used. The broad peak at $2\theta = 10°$ observed in the XRD scattering pattern corresponds to GO while the peak at $2\theta = 20°$ is due to the poly(S−BA) copolymer.[63] The average interlayer distance of the GO in the nanocomposites was 0.84 nm, which is greater than that of the as-prepared GO (0.74 nm) and AMPS-modified GO (0.80 nm). This indicates that AMPS plays a very important role in the intercalation process of graphene oxide platelets during polymerization.

Figure 9 shows that at AMPS-GO loadings of 1−4% the nanocomposite resulted in mainly intercalated structure. This is indicated by a broad peak that emerged at a 2θ value of ∼10°, which is lower than that of GO and AMPS-GO (see XRD results in Figure 6). In the case that an intercalated morphology is formed, few polymer chains can penetrate between the GO nanogalleries; thus, the interlayer distance is increased. This leads to a shift of the diffraction peak toward lower angle values in the XRD pattern.[64] However, when the AMPS-GO loading was relatively high (5−6%), the nanostructure showed more exfoliated morphology, indicated by a less defined peak.[65] Similar results obtained for polymer composites made with other filler materials such as clay,[49] which were attributed to thermodynamic effects. In the presence of high filler content, the filler particles are very close to each other, and any particle movements can generate energy by friction. This energy could lead to a free movement of other filler particles, resulting in a random

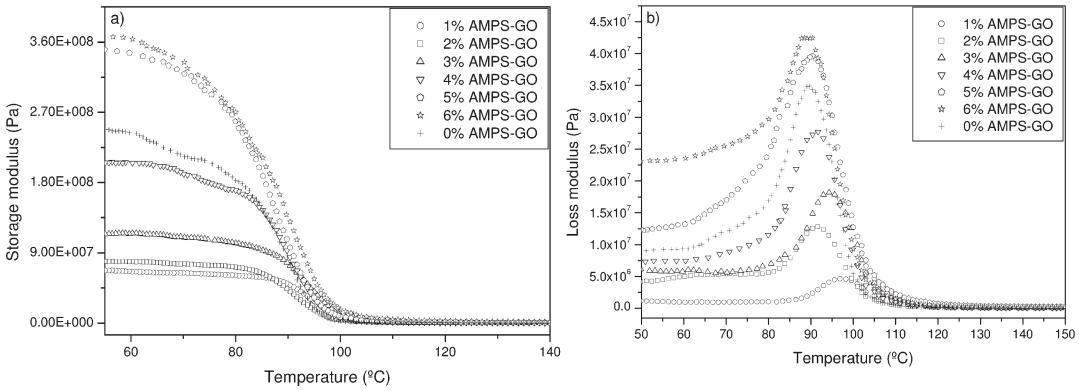

Figure 10. Mechanical properties as a function of temperature of poly(S−BA)/GO nanocomposites, at graphite loadings of 0−6 wt %: (a) storage modulus and (b) loss modulus.

Table 3. T_g Values of Poly(S−BA)/GO Nanocomposites, at Graphite Loadings of 0−6 wt %

nanocomposite	AMPS-GO content (wt %)	T_g (°C)
P(S−BA)	0	87.0
P(S−BA)/GO-1	1	94.5
P(S−BA)/GO-2	2	89.0
P(S−BA)/GO-3	3	92.0
P(S−BA)/GO-4	4	89.0
P(S−BA)/GO-5	5	88.0
P(S−BA)/GO-6	6	89.0

orientation of these particles (i.e., a less defined peak in the XRD will be observed).[65]

3.3.3. Mechanical Properties of the Poly(S−BA)/GO Nanocomposites. The mechanical properties of poly(S−BA)/GO nanocomposites were determined by DMA. Measurements were performed on the dried films prepared from the poly(S−BA)/GO latices containing 0−6 wt % GO relative to monomer. DMA analysis showed that the nanocomposites with high GO content had enhanced storage and loss modulus in the glassy state relative to the neat poly(S−BA) standard (see Figure 10). At graphite loadings of 1−4% relative to monomer the storage and loss modulus of the nanocomposites was lower than that of the poly(S−BA) standard (0% GO) (2.5×10^8 and 9.0×10^6 Pa, respectively). However, samples with higher graphite content (5 and 6%) had higher storage and loss modulus values than the poly(S−BA) standard. Furthermore, it was noted that the storage and loss modulus of poly(S−BA)/GO nanocomposites increased with increasing AMPS-GO content in the sample. As indicated in the XRD results in Figure 9, when the AMPS-GO loading increased, the degree of graphene exfoliation was enhanced significantly. This resulted in the formation of polymer nanocomposites with improved mechanical properties (i.e., improved storage and loss modulus).

The glass transition temperature (T_g) of the polymer in a nanocomposite was determined from the onset temperature of the tan δ curve in the DMA scan. The variation of tan δ of the poly(S−BA)/GO nanocomposites with temperature is shown in Figure S2 of the Supporting Information. It was noticed that the area of the tan δ peak of the nanocomposite is smaller than that of the neat poly(S−BA) copolymer. This was due to the incorporation of polymer chains inside the graphite galleries, which led to reduced damping.[66] Table 3 shows the T_g values of all nanocomposites synthesized with different GO content (0−6 wt %). The T_g of poly(S−BA) was enhanced in the presence of AMPS-modified GO relative to composites made with 0% GO.

Table 4. $\overline{M}_n$, $\overline{M}_w$, and PDI of the Poly(S−BA) Standard and Poly(S−BA)/GO Nanocomposites Prepared Using Different Quantities of GO (0−6 wt %)

nanocomposite	AMPS-GO content (wt %)	$\overline{M}_n$ (g/mol)	$\overline{M}_w$ (g/mol)	PDI
P(S−BA)	0	7.1×10^5	1.5×10^6	2.1
P(S−BA)/GO-1	1	5.2×10^5	1.6×10^6	3.2
P(S−BA)/GO-2	2	4.0×10^5	1.3×10^6	3.3
P(S−BA)/GO-3	3	3.6×10^5	1.2×10^6	3.4
P(S−BA)/GO-4	4	3.6×10^5	1.1×10^6	3.2
P(S−BA)/GO-5	5	2.6×10^5	8.4×10^5	3.2
P(S−BA)/GO-6	6	2.7×10^5	7.7×10^5	2.8

However, the increase in T_g was not a function of AMPS-GO content in the composites. This was rather surprising because an increase in GO content is expected to result in nanocomposites with increased T_g values. This behavior was attributed to the change in molecular weight of the polymer chains caused by the presence of graphite. This can be seen in Table 4, which tabulates the molar masses (weight average molecular weight, $\overline{M}_w$, and number average molecular weight, $\overline{M}_n$) and polydispersity index (PDI) of the poly(S−BA) standard and poly(S−BA)/GO nanocomposites prepared using different quantities of AMPS-GO. As the graphite loading increased, the molecular weight of the copolymer decreased markedly, especially in the case of 2, 5, and 6% AMPS-GO loadings. However, the PDI of poly(S−BA) copolymer was slightly affected by the change in graphite concentration. The low molecular weight polymer chains may act as plasticizer and cause the T_g of the polymer in the nanocomposite to decrease.[67] This plasticization effect could counteract the effect of AMPS-GO on the polymer chain movements, resulting in less improvement in the T_g.

Similar results were observed for polymer nanocomposites made with other fillers, such as clay. Greesh et al.[68] observed that clay loading had a significant effect on the molecular weight of poly(S−BA) nanocomposites prepared by emulsion polymerization. They found that the molecular weight of poly(S−BA) decreased as the clay concentration increased in the nanocomposites. They

dx.doi.org/10.1021/ma2003008 |*Macromolecules* 2011, 44, 8504–8515

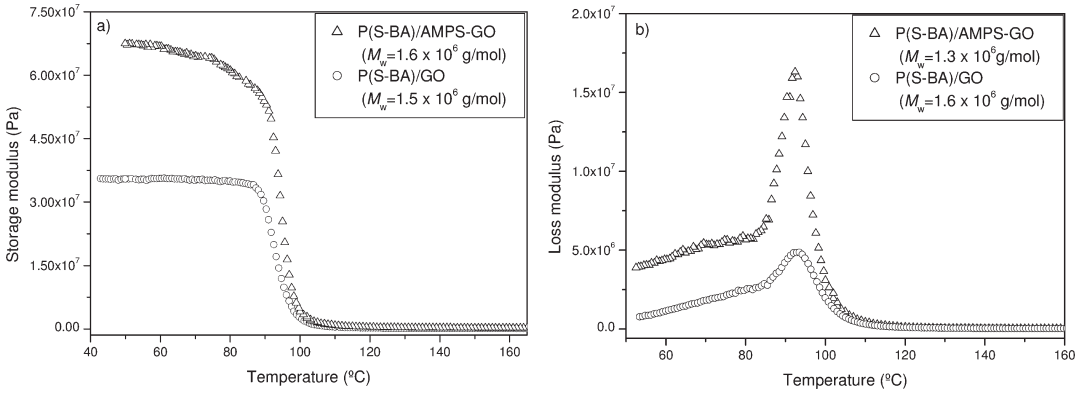

Figure 11. Mechanical properties as a function of temperature of poly(S−BA) nanocomposites made with AMPS-GO and GO: (a) storage modulus (1 wt % of filler loading) and (b) loss modulus (2 wt % of filler loading).

attributed these results to the presence of clay particles, which may hinder the growth of polymer chains, resulting in a decreased molecular weight as the clay concentration increases. Due to the dispersion of the filler particles in the monomer phase, the viscosity increases; thus, the movement and diffusivity of the monomers, initiators, and free radicals may all be retarded. Therefore, the probability of chain propagation, chain transfer, and termination decreases with increasing filler content.[69]

The improvement in mechanical properties of poly(S−BA) in the presence of AMPS-modified GO is because of the fine dispersion of the nanosheets and strong interaction between the polar groups of poly(S−BA) and the polar groups of GO. These GO nanoplatelets have a high aspect ratio (due to the high exfoliation of GO nanosheets), which greatly restricts the mobility of the polymer chain segments near the polymer−graphite interface, resulting in higher storage and loss modulus and T_g values.[66,70] Furthermore, the modification of GO with AMPS widened the interlayer spacing between the graphene layers and facilitated the intercalation of monomers into the GO nanogalleries. This led to the formation of poly(S−BA) nanocomposites with exfoliated structure, leading to enhanced mechanical properties.

The effect of GO modification with AMPS can be seen in Figure 11, which shows the mechanical properties (storage and loss modulus) of composite samples made with AMPS-modified GO and unmodified GO. The mechanical properties are significantly improved in composites made with AMPS-modified GO, compared to those made with the neat GO. The storage modulus increased from 3.5×10^7 to about 6.7×10^7 Pa, while the loss modulus increased from 1.0×10^6 to about 4.3×10^6 Pa. This indicates that the improvement in mechanical properties is due to the modification of GO with AMPS, which resulted in largely exfoliated graphene nanosheets dispersed in the polymer matrix.

Table 3 shows that the highest T_g value is observed when the graphite loading is 1%. This seems to be the threshold at which the best interaction between the graphite nanosheets and the polymer occurs. It should be noted here that the storage and loss modulus values were not the highest when 1 wt % AMPS-GO loading was used. This can be attributed to the changes in mechanical behavior of a polymer sample as a function of temperature. The storage and loss modulus are a measure of the elastic and plastic response of a polymer to the deformation as a function of temperature, respectively. On the other hand, the

Table 5. Thermogravimetric Properties of Poly(S−BA) and Its Nanocomposites Made with Different Concentrations of GO (0−6 wt %)

nanocomposite	AMPS-GO loading (wt %)	$T_{10\%}$ (°C)	$T_{90\%}$ (°C)	char (%)
P(S−BA)	0	415.0	459.5	0.24
P(S−BA)/GO-1	1	433.5	490.0	1.09
P(S−BA)/GO-2	2	435.5	492.5	1.71
P(S−BA)/GO-3	3	428.0	483.0	2.15
P(S−BA)/GO-4	4	426.0	487.5	2.69
P(S−BA)/GO-5	5	421.0	483.0	4.10
P(S−BA)/GO-6	6	423.0	489.0	4.15

T_g is used to measure the molecular mobility of polymers as a function of temperature. The intercalation with even small amounts of graphene nanosheets will lead to a restricted mobility of polymer chains, resulting in higher T_g.

3.3.4. Thermal Stability of Poly(S−BA)/GO Nanocomposites. Yet another enhanced property that polymer/graphite nanocomposites may exhibit is their increased thermal stability compared to neat polymers.[71,72] Our results showed that the thermal stability of poly(S−BA)/GO nanocomposites was improved, relative to neat poly(S−BA) copolymer. The TGA thermograms of poly(S−BA)/GO nanocomposites prepared with different quantities of modified GOs are shown in Figure S3 of the Supporting Information. Table 5 tabulates the thermogravimetric data, including T_{10} and T_{90} of degradation. T_{10} is the onset temperature at which 10% degradation of the nanocomposite occurs, and T_{90} is the temperature at which 90% degradation occurs. The remaining fraction of nonvolatile material left at 850 °C, called char, is also shown in Table 5. The poly(S−BA) copolymer does not contain any volatile products below 395 °C; however, the main chain of poly(S−BA) decomposes at around 400 °C.

Table 5 shows that all nanocomposites synthesized with AMPS-modified GO are more thermally stable relative to the neat poly(S−BA) copolymer. At graphite loading of only 1−2% relative to monomer the temperature of degradation of the nanocomposite increased, relative to pure polymer. The T_{10} of all the synthesized nanocomposite increased by 6−20.5 °C compared to pure poly(S−BA) copolymer, and T_{90} increased by about 23.5−33.0 °C. This clearly shows that the thermal stability of poly(S−BA) increases in the presence of AMPS-GO.

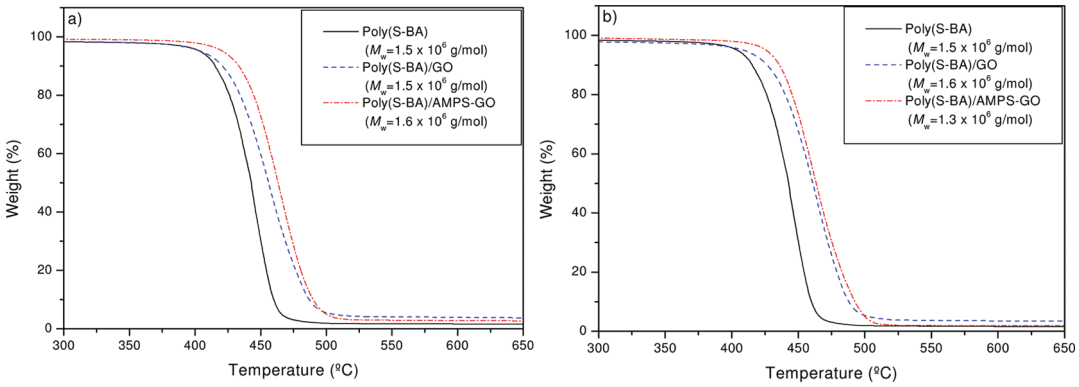

Figure 12. Thermal properties as a function of temperature of poly(S−BA) nanocomposites made with AMPS-GO and GO: (a) 1 wt % AMPS-GO and GO loading and (b) 2 wt % AMPS-GO and GO loading.

However, a further increase in graphite loading did not result in any improvement of thermal stability relative to the case of graphite loading of 1−2%. Moreover, the increase in graphite content above 2% in the nanocomposites generally resulted in a slight decrease in the thermal stability of the nanocomposites. This can be explained by the effect of graphite loading on the molecular weight of the copolymer, as seen in Table 4. As the graphite content increased in the nanocomposite, there was a significant decrease in the molecular weight of the copolymer. The change in molecular weight may counteract the effect of the increase in graphite loading on the thermal stability of the nanocomposites. Samakande et al.[73] observed the same effect of the filler content on the thermal stability of PS made with clay nanoparticles.

The TGA data in Table 5 also show that at 850 °C, when the residue of pure polymer is 0.24%, the charred residue of the nanocomposites is increased with increasing AMPS-GO loadings. These results indicate that introducing GO into the nanocomposites enhances the formation of char on the surface of the polymer and, consequently, reduces the rate of decomposition.[64] It should be noted here that at AMPS-GO loading of 3−6 wt % the char was significantly lower than the nominal amount of modified GO that was added. This is because the graphene nanosheets in these nanocomposites are largely exfoliated. We hypothesize that the exfoliated nanosheets (especially the single sheets) will not form char as the stacked graphene sheets do. The exfoliated sheets will burn more easily than the intercalated or less exfoliated ones. Therefore, a significant difference between the nominal and the actual char content will be observed. The difference in char content could be the reason why some composites did not exhibit increased thermal stability relative to the case of composites with 1−2 wt % filler loadings. It should be also noted that at 6% AMPS-GO loading the char content is similar to that of the 5% AMPS-GO loading sample (see Table 5); subsequently, these nanocomposites exhibit similar T_g values of 89 and 88 °C, respectively.

TGA results also proved that there is a significant enhancement in thermal stability when the GO was modified with AMPS. Figure 12 shows the thermal properties of composite samples made with AMPS-modified GO and unmodified GO. For comparison, the TGA curve of the poly(S−BA) standard is also shown in Figure 12. It is clear that the thermal properties are significantly improved in composites made with AMPS-modified GO, compared to those made with the neat GO. At a filler loading of 1%, the T_{10} and T_{90} increased from 421.5 to 433.5 °C and 486.0 to 490.0 °C, respectively. Similarly, at graphite loading of 2%, the T_{10} and T_{90} increased from 426.0 to 436.0 °C and 487.0 to 493.0 °C, respectively. This indicates that AMPS plays a very significant role in the exfoliation of graphene oxide in the polymer matrix, which results in largely exfoliated nanocomposites with improved thermal stability.

4. CONCLUSION

A novel method was demonstrated for the preparation of exfoliated poly(S−BA)/GO nanocomposites using the miniemulsion polymerization technique. The synthesis was carried out by first mixing the GO with AMPS, followed by miniemulsification in the presence of St and BA monomers. The polymerization resulted in encapsulated graphene oxide nanosheets in poly(S−BA) particles, and the nanocomposites were exfoliated during polymerization. TEM showed that the graphene nanosheets were exfoliated (∼2−5 layers thick) in the films obtained from the synthesized nanocomposite latices. TEM also revealed that dispersion of graphene nanosheets covered with a copolymer layer in an encapsulated structure, with good particle size distribution, was achieved.

The exfoliated structure in the nanocomposites was confirmed by XRD measurements. The nanocomposites had structures ranging from intercalated to largely exfoliated, and the degree of graphene exfoliation was enhanced as the AMPS-GO loading increased. The modification of GO with AMPS broadened the gap between the graphene layers and facilitated the intercalation of monomers into the GO nanogalleries. This provided the needed exfoliation driving force for the formation of poly(S−BA) nanocomposites with exfoliated structure. The use of miniemulsion as the *in situ* polymerization method promoted the intercalation of St and BA monomers into the modified GO layers.

TGA and DMA analyses indicated that polymer nanocomposites prepared with AMPS-modified GO had better thermal and mechanical properties relative to the neat polymer. Furthermore, the use of AMPS-GO led to the synthesis of nanocomposites with better properties compared to those synthesized with unmodified GO (i.e., as-prepared GO). DMA proved that the mechanical properties of poly(S−BA), namely storage and loss modulus, increased in the presence of AMPS-GO, as a function of filler loading. Moreover, all nanocomposites made with AMPS-GO had T_g values higher than that of the neat poly(S−BA) copolymer. However, the increase in the T_g of the

copolymer was not a function of filler content. This was attributed to the effect of modified GO concentration on the molecular weight of the polymer, which showed a significant decrease as the filler content increased. TGA results also indicated that all the prepared nanocomposites exhibited enhanced thermal stability in the presence of AMPS-modified GO compared to the neat copolymer. The thermal decomposition of all nanocomposites shifted to higher temperature in the presence of AMPS-modified GO relative to the neat copolymer.

■ ASSOCIATED CONTENT

Supporting Information. Figures S1−S3. This material is available free of charge via the Internet at http://pubs.acs.org.

■ AUTHOR INFORMATION

Corresponding Author
*E-mail: hmetmimi@gmail.com.

■ ACKNOWLEDGMENT

Financial support from the International Center for Macromolecular Chemistry and Technology in Libya is gratefully acknowledged.

■ REFERENCES

(1) Stankovich, S.; Dikin, D. A.; Dommett, G. H.; Kohlhaas, K. M.; Zimmney, E. J.; Stach, E. A.; Piner, R. D.; Nguyen, S. T.; Ruoff, R. S. *Nature* **2006**, *442*, 282–286.
(2) Geim, A. K.; Novoselov, K. S. *Nature Mater.* **2007**, *6* (3), 183–191.
(3) Dreyer, D. R.; Ruoff, R. S.; Bielawski, C. W. *Angew. Chem., Int. Ed.* **2010**, *49* (49), 9336–9344.
(4) Lee, C.; Wei, X.; Kysar, J. W.; Hone, J. *Science* **2008**, *321* (5887), 385–388.
(5) Velasco-Santos, C.; Martinez-Hernandez, A. L.; Castano, V. M. *Compos. Interfaces* **2005**, *11* (8/9), 567–586.
(6) Viculis, L. M.; Mack, J. J.; Mayer, O. M.; Hahn, H. T.; Kaner, R. B. *J. Mater. Chem.* **2005**, *15*, 974–978.
(7) Kim, H.; Abdala, A. A.; Macosko, C. W. *Macromolecules* **2010**, *43* (16), 6515–6530.
(8) Wakabayashi, K.; Pierre, C.; Dikin, D. A.; Ruoff, R. S.; Ramanathan, T.; Brinson, L. C.; Torkelson, J. M. *Macromolecules* **2008**, *41* (6), 1905–1908.
(9) Dreyer, D. R.; Park, S.; Bielawski, C. W.; Ruoff, R. S. *Chem. Soc. Rev.* **2010**, *39* (1), 228–240.
(10) Schniepp, H. C.; Li, J.-L.; McAllister, M. J.; Sai, H.; Herrera-Alonso, M.; Adamson, D. H.; Prud'homme, R. K.; Car, R.; Saville, D. A.; Aksay, I. A. *J. Phys. Chem. B* **2006**, *110* (17), 8535–8539.
(11) Stankovich, S.; Piner, R. D.; Chen, X.; Wu, N.; Nguyen, S. T.; Ruoff, R. S. *J. Mater. Chem.* **2006**, *16* (2), 155–158.
(12) Brodie, B. C. *Philos. Trans. R. Soc. London, A* **1859**, *149*, 249–259.
(13) Staudenmaier, L. *Ber. Dtsch. Chem. Ges.* **1898**, *31*, 1481–1487.
(14) Hummers, W. S.; Offeman, R. E. *J. Am. Chem. Soc.* **1958**, *80*, 1339.
(15) He, H.; Klinowski, J.; Forster, M.; Lerf, A. *Chem. Phys. Lett.* **1998**, *287* (1−2), 53–56.
(16) Lerf, A.; He, H.; Forster, M.; Klinowski, J. *J. Phys. Chem. B* **1998**, *102* (23), 4477–4482.
(17) Hontoria-Lucas, C.; López-Peinado, A. J.; López-González, J. d. D.; Rojas-Cervantes, M. L.; Martín-Aranda, R. M. *Carbon* **1995**, *33* (11), 1585–1592.
(18) He, H.; Riedl, T.; Lerf, A.; Klinowski, J. *J. Phys. Chem.* **1996**, *100* (51), 19954–19958.
(19) Szabó, T.; Szeri, A.; Dékány, I. *Carbon* **2005**, *43* (1), 87–94.
(20) Hirata, M.; Gotou, T.; Horiuchi, S.; Fujiwara, M.; Ohba, M. *Carbon* **2004**, *42* (14), 2929–2937.
(21) Hirata, M.; Gotou, T.; Ohba, M. *Carbon* **2005**, *43* (3), 503–510.
(22) Titelman, G. I.; Gelman, V.; Bron, S.; Khalfin, R. L.; Cohen, Y.; Bianco-Peled, H. *Carbon* **2005**, *43* (3), 641–649.
(23) Putz, K. W.; Compton, O. C.; Palmeri, M. J.; Nguyen, S. T.; Brinson, L. C. *Adv. Funct. Mater.* **2010**, *20* (19), 3322–3329.
(24) Wang, W.-P.; Pan, C.-Y. *Polym. Eng. Sci.* **2004**, *44* (12), 2335–2339.
(25) Potts, J. R.; Dreyer, D. R.; Bielawski, C. W.; Ruoff, R. S. *Polymer* **2011**, *52* (1), 5–25.
(26) Hu, H.; Wang, X.; Wang, J.; Wan, L.; Liu, F.; Zheng, H.; Chen, R.; Xu, C. *Chem. Phys. Lett.* **2010**, *484* (4−6), 247–253.
(27) Savoskin, M. V.; Yaroshenko, A. P.; Whyman, G. E.; Mysyk, R. D. *J. Phys. Chem. Solids* **2006**, *67*, 1127–1131.
(28) Du, X. S.; Xiao, M.; Meng, Y. Z. *J. Polym. Sci., Part B: Polym. Phys.* **2004**, *42*, 1972–1978.
(29) Kim, T. Y.; Lee, H. W.; Stoller, M.; Dreyer, D. R.; Bielawski, C. W.; Ruoff, R. S.; Suh, K. S. *ACS Nano* **2011**, *5* (1), 436–442.
(30) Zheng, W.; Wong, S.-C. *Compos. Sci. Technol.* **2003**, *63* (2), 225–235.
(31) Jing-Wei, S.; Xiao-Mei, C.; Wen-Yi, H. *J. Appl. Polym. Sci.* **2003**, *88* (7), 1864–1869.
(32) Wenge, Z.; Xuehong, L.; Shing-Chung, W. *J. Appl. Polym. Sci.* **2004**, *91* (5), 2781–2788.
(33) Liu, P.-G.; Xiao, P.; Xiao, M.; Gong, K.-c. *Chin. J. Polym. Sci.* **2000**, *18* (5), 413–418.
(34) Zheng, G.; Wu, J.; Wang, W.; Pan, C. *Carbon* **2004**, *42*, 2839–2847.
(35) Samakande, A.; Sanderson, R. D.; Hartmann, P. C. *J. Polym. Sci., Part A: Polym. Chem.* **2008**, *46* (21), 7114–7126.
(36) Lu, H. F.; Fei, B.; Xin, J. H.; Wang, R. H.; Li, L.; Guan, W. C. *Carbon* **2007**, *45* (5), 936–942.
(37) Etmimi, H. M.; Tonge, M. P.; Sanderson, R. D. *J. Polym. Sci., Part A: Polym. Chem.* **2011**, *49* (7), 1621–1632.
(38) El-Aasser, M.; Sudol, E. Features of Emulsion Polymerization. In *Emulsion Polymerization and Emulsion Polymers*, 2nd ed.; Lovell, P., El-Aasser, M., Eds.; John Wiley & Sons Ltd.: New York, 1997; pp 37−58.
(39) Schork, F.; Poehlein, G.; Wang, S.; Reimers, J.; Rodrigues, J.; Samer, C. *Colloids Surf., A* **1999**, *153*, 39–45.
(40) Sudol, E.; El-Aasser, M. Miniemulsion Polymerization. In *Emulsion Polymerization and Emulsion Polymers*, 2nd ed.; Lovell, P., El-Aasser, M., Eds.; John Wiley & Sons Ltd.: New York, 1997; pp 699−722.
(41) Schork, F. J.; Luo, Y.; Smulders, W.; Russum, J. P.; Butte, A.; Fontenot, K. *Adv. Polym. Sci.* **2005**, *175*, 129–255.
(42) Ugelstad, J.; El-Aasser, M.; Vanderhoff, J. *J. Polym. Sci., Polym. Lett. Ed.* **1973**, *11*, 503–513.
(43) Landfester, K.; Bechthold, N.; Forster, S.; Antonietti, M. *Macromol. Rapid Commun.* **1999**, *20*, 81–84.
(44) Miller, C.; Sudol, E.; Silebi, C.; El-Aasser, M. *J. Polym. Sci., Part A: Polym. Chem.* **1995**, *33*, 1391–1408.
(45) Wu, X.; Schork, F. *Ind. Eng. Chem. Res.* **2000**, *39*, 2855–2865.
(46) Asua, J. *Prog. Polym. Sci.* **2002**, *27*, 1283–1346.
(47) Xu, M.; Choi, Y. S.; Kim, Y. K.; Wang, K. H.; Chung, I. J. *Polymer* **2003**, *44* (20), 6387–6395.
(48) Choi, Y. S.; Ham, H. T.; Chung, I. J. *Polymer* **2003**, *44* (26), 8147–8154.
(49) Choi, Y. S.; Ham, H. T.; Chung, I. J. *Chem. Mater.* **2004**, *16* (13), 2522–2529.
(50) Greesh, N.; Hartmann, P. C.; Cloete, V.; Sanderson, R. D. *J. Colloid Interface Sci.* **2008**, *319* (1), 2–11.
(51) Uhl, F. M.; Wilkie, C. A. *Polym. Degrad. Stab.* **2004**, *84* (2), 215–226.
(52) Uhl, F. M.; Yao, Q.; Nakajima, H.; Manias, E.; Wilkie, C. A. *Polym. Degrad. Stab.* **2005**, *89* (1), 70–84.

(53) Wang, W. P.; Liu, Y.; Li, X. X.; You, Y. Z. *J. Appl. Polym. Sci.* **2006**, *100* (2), 1427–1431.
(54) Chung, D. *J. Mater. Sci.* **1987**, *22* (12), 4190–4198.
(55) Mai, Y.-W.; Yu, Z.-Z. *Polymer Nanocomposites*, 1st ed.; Woodhead Publishing Limited: New York, 2006; Vol. 19, pp 510−533.
(56) Bourlinos, A. B.; Gournis, D.; Petridis, D.; Szabo, T.; Szeri, A.; Dekany, I. *Langmuir* **2003**, *19* (15), 6050–6055.
(57) Nethravathi, C.; Rajamathi, M. *Carbon* **2006**, *44* (13), 2635–2641.
(58) Bhinde, T.; Clarke, S. M.; Phillips, T. K.; Arnold, T.; Parker, J. E. *Langmuir* **2010**, *26* (11), 8201–8206.
(59) Bragg, W. L. *Proc. Cambridge Philos. Soc.* **1913**, *17*, 43–57.
(60) Vaia, R. A.; Teukolsky, R. K.; Giannelis, E. P. *Chem. Mater.* **1994**, *6* (7), 1017–1022.
(61) Choi, K. S.; Liu, F.; Choi, J. S.; Seo, T. S. *Langmuir* **2010**, *26* (15), 12902–12908.
(62) Stankovich, S.; Piner, R. D.; Nguyen, S. T.; Ruoff, R. S. *Carbon* **2006**, *44* (15), 3342–3347.
(63) Zhang, R.; Hu, Y.; Xu, J.; Fan, W.; Chen, Z. *Polym. Degrad. Stab.* **2004**, *85* (1), 583–588.
(64) Ding, R.; Hu, Y.; Gui, Z.; Zong, R.; Chen, Z.; Fan, W. *Polym. Degrad. Stab.* **2003**, *81* (3), 473–476.
(65) Meng, Y. Polymer/Graphite Nanocomposites. In *Polymer Nanocomposites*, 2nd ed.; Mai, Y.-W., Yu, Z.-Z., Eds.; Woodhead Publishing Limited: Cambridge, 2006; Vol. 19, pp 510−539.
(66) Yang, J.; Tian, M.; Jia, Q.-X.; Shi, J.-H.; Zhang, L.-Q.; Lim, S.-H.; Yu, Z.-Z.; Mai, Y.-W. *Acta Mater.* **2007**, *55* (18), 6372–6382.
(67) Wang, C.; Wang, Q.; Chen, X. *Macromol. Mater. Eng.* **2005**, *290* (9), 920–926.
(68) Greesh, N.; Hartmann, P. C.; Sanderson, R. D. *Macromol. Mater. Eng.* **2009**, *294* (3), 206–212.
(69) Zhong, Y.; Zhu, Z.; Wang, S.-Q. *Polymer* **2005**, *46* (9), 3006–3013.
(70) Donghwan, C.; Sangyeob, L.; Gyeongmo, Y.; Hiroyuki, F.; Lawrence, T. D. *Macromol. Mater. Eng.* **2005**, *290* (3), 179–187.
(71) Xiao, M.; Sun, L.; Liu, J.; Li, Y.; Gong, K. *Polymer* **2002**, *43* (8), 2245–2248.
(72) Uhl, F. M.; Wilkie, C. A. *Polym. Degrad. Stab.* **2002**, *76* (1), 111–122.
(73) Samakande, A.; Sanderson, R. D.; Hartmann, P. C. *Eur. Polym. J.* **2009**, *45* (3), 649–657.